PAPER • OPEN ACCESS

# Enzymatic and catalytic behaviour of low-dimensional gold nanomaterials in modular nano-composite hydrogels

Materials Research Express

PAPER

# Enzymatic and catalytic behaviour of low-dimensional gold nanomaterials in modular nano-composite hydrogels

George Newham, Joseph Fox, Samuel C T Moorcroft and Stephen D Evans*

School of Physics and Astronomy, University of Leeds, Woodhouse Lane, LS2 9JT, United Kingdom

* Author to whom any correspondence should be addressed.

E-mail: s.d.evans@leeds.ac.uk

OPEN ACCESS

RECEIVED
20 February 2023

REVISED
24 May 2023

ACCEPTED FOR PUBLICATION
6 June 2023

PUBLISHED
14 June 2023

Keywords: enzymatic, catalytic, behaviour, low-dimensional, gold, nanomaterials



## Abstract

Inorganic nanoparticles have long been applied as catalysts and nanozymes with exceptional rate constants arising from their large surface areas. While it is understood that high surface area-to-volume ratios and low average atomic coordination are responsible for their exceptional catalytic properties, these facets remain under exploited in the design of gold nanoparticle catalysts and nanozymes. Here we have developed 3D, 2D, and quasi-1D gold nanoparticles for use as catalysts in reducing 4-nitrophenol by sodium borohydride. Each morphology was characterised with transmission electron microscopy and UV–vis absorption spectroscopy, while the highest catalytic activity was achieved when the perimeter-to-surface area, or amount of 'edge', was maximised. The particles were then applied as nanozymes in modular nano-composite hydrogels. Independent hydrogel tiles containing either the substrate or catalyst were bonded in stacks, which allowed reagent transport across their interface for the colourimetric detection of hydrogen peroxide. This work presents novel insight into the catalytic activity of low-dimension nanoparticles and their potential application in nanozyme-based diagnostic devices.

## 1. Introduction

Nanozymes are a class of inorganic nanomaterials that can mimic the activity of enzymes. They have attracted significant attention in research, largely due to their stability, ease of storage, reusability, and relatively low cost, all of which are pitfalls of their traditional biological counterparts. Since the first reports of peroxide-mimicking behavior [1], the permissible enzymatic reactions performed by nanozymes has grown to include oxidases, catalases, uricases, hydrolases, and others [2, 3]. Further, the range of nanomaterials known to exhibit this behaviour has also increased enormously, including but not limited to gold [4], iron oxide [5], platinum [6], and copper [7].

Ye *et al* recently reported the synthesis of freestanding, atomically thin gold nanosheets (AuNS) for the first time, whose 2D nature imparted exceptional catalytic activity for the reduction of 4-nitrophenol by sodium borohydride. The AuNS also exhibited peroxide-mimicking behaviour with substrate 3,3′,5,5′-tetramethylbenzidine (TMB) over a wide range of pH and temperatures [8]. Lower dimensional nanostructures (e.g. 2D sheets and quasi-1D tapes) possess higher surface area-to-volume ratios than conventionally used 3D nanospheres, and their high perimeter-to-surface area ratios increase the number of low-coordination atoms, both of which are known to benefit catalytic activity [9]. However, the control of dimensionality as a means of tuning catalytic and nano-enzymatic activity remains under-exploited. Herein, we extend the previously reported synthesis of 2D AuNS to produce 3D superstructures with pinecone-like morphology (AuNPC), and quasi-1D nano-Tapes (AuNT). We then demonstrate the beneficial effect of decreased dimensionality on nanoparticle catalysis with 3D, 2D, and 1D gold nanoparticles in the model reduction of 4-nitrophenol by sodium borohydride.

The repeated use of nanomaterials as homogenous catalysts or enzymes requires the separation and collection of the catalyst for re-use, which may be non-trivial. In addition, the necessity of the liquid phase for

reaction limits their potential application to laboratory settings. However, incorporating nanomaterials into macroscale hydrogels can retain their catalytic properties and permit their function as heterogeneous catalysts where the reaction mix may diffuse through the porous hydrogel and react with nanoparticles immobilised in the polymer matrix [10, 11]. This can be applied as a flow-through reactor with a driven flow of the reaction mixture through a nanocomposite membrane or simply with the hydrogel placed in a reaction solution; in each case, the catalyst may be readily reused [12]. By extension, these reactions need not occur on the laboratory bench-top and have been applied as wound dressings or injectable therapeutics, where wound fluid may diffuse into, and from, the hydrogel for the nano-enzymatic reduction of reactive oxygen species, which in turn promotes healing [13–15]. They also show great potential as portable sensors, particularly nano-enzymatically driven colourimetric assays for the environmental detection of analytes settings by the naked eye [16, 17].

To date, most reported examples of nano-enzymatic composite hydrogels contain each reagents in a single hydrogel. Herein we report a facile and unique modular design for the colourimetric detection of hydrogen peroxide. Peroxidase-mimicking, quasi-1D gold nanozymes and the colourimetric substrate (diaminobenzidine; DAB) were prepared separately in physical polyvinyl alcohol (PVA) hydrogel 'tiles' and then layered and healed together into a robust single vertical 'stack'. The healing of the tiles is such that diffusion of hydrogen peroxide up through the stack carries the DAB substrate into the upper nanozyme-containing layer, where the enzymatic oxidation of the substrate yields a visible colour change. The colour change was clearly visible to the eye and was highly sensitive to the hydrogen peroxide concentration.

We present this firstly as a portable colourimetric assay, but secondly as a proof-of-concept for a wider system in which multiple reagents may be prepared in separate hydrogel tiles and then combined into a mechanically robust single nanocomposite stack.

## 2. Materials and methods

### 2.1. Materials

Gold chloride trihydrate, 4-nitrophenol, citric acid, sodium phosphate dibasic, and poly(vinyl alcohol)_(PVA; $M_w$ 146–148 kDa; 99%+ hydrolysed) were purchased from Sigma Aldrich. Trisodium citrate, methyl orange, and 3,3′-Diaminobenzidine (DAB) were purchased from Alfa Aesar. Sodium borohydride, hydrogen peroxide, and hydrochloric acid were purchased from Fisher Scientific. All chemicals were of analytical grade and used without further purification. Ultrapure water (Millipore Milli-Q) with 18.2 MΩ cm resistivity at 25 °C was used in all experiments.

### 2.2. Synthesis of AuNX

The synthesis procedures presented herein are adapted from publications by Ye *et al* [8] and Fox *et al* [18] for the formation of 2D AuNS, and expanded by our group to also produce quasi-1D and 3D morphologies. For the preparation of 3D gold nano-pinecones (AuNPC), 40 ml of 2.5 mm methyl orange, 10 ml of 5 mm gold chloride, and 5 ml of 150 mm sodium citrate were sequentially added to a glass vial at room temperature. After 30 min, the product was collected and rinsed thrice by centrifugation at 4,600 g for 10 min and resuspension. The final AuNPC solution was dispersed in ultrapure water. For the synthesis of 2D gold nanosheets (AuNS), 4 ml of 0.21 mm methyl orange, 1 ml of 5 mm gold chloride, and 500 $\mu$l of 100 mm sodium citrate were added sequentially to a glass vial at 4 °C and maintained at this temperature overnight [18]. The sediment was collected from the vial and cleaned by centrifugation at 1,000 g for 10 min and rinsed thrice before dispersion in ultrapure water. For the synthesis of quasi-1D gold nano-tapes (AuNT) the same synthesis protocol was followed as for the 2D AuNS, but at room temperature, after which no sediment was observed, and the product was collected and rinsed by centrifugation at 3,000 g for 60 min.

### 2.3. Characterisation of the AuNX

The morphology of the AuNX was characterisation using high-resolution TEM (FEI tecnai G2-Spirit) with an accelerating voltage of 120 kV and a Gatan ultrascan 4000 CCD camera. To prepare for imaging, 5 $\mu$l of the as-prepared sample was dried onto a carbon-coated copper grid. The particle size distributions, surface areas, and perimeters were assessed from the TEM images using ImageJ analysis software. The UV–vis extinction spectra were collected with the Agilent Cary 5000. 1 ml of sample was analysed using Brand Micro UV cuvettes with a 10 mm path length.

### 2.4. Catalytic testing of the AuNX

The catalytic performance of the AuNX was tested against the reduction of 4-nirophenol by sodium borohydride. 10 $\mu$l of 15 mm 4-NP, 980 $\mu$l of 20 mm sodium borohydride, and 10 $\mu$l of 900 $\mu$g ml$^{-1}$ AuNX solution were combined in a cuvette (path length 10 mm) at 20 °C. UV–vis spectra were collected every 5 min,

and the reaction kinetics were monitored by the optical absorbance at 400 nm. The rate constants were calculated assuming pseudo first-order kinetics (equation (1)):

$$k_{app}t = \ln\left(\frac{C_0}{C_t}\right) \tag{1}$$

where $k_{app}$ is the apparent rate constant, $t$ is time, and $C_0$ and $C_t$ are the concentrations of 4-nitrophenol at time *0* and time *t*. The apparent rate constant ($k_{app}$) was determined from the slope of the linear region of a plot of $\ln(C_0/C_t)$ versus *t*, where $C_0$ and $C_t$ were given by the 400 nm absorbance at time *0* and *t*, $A_0$ and $A_t$, respectively. Each data point was the average ± standard deviation of 3 repeats.

The mass normalised rate constant ($k_1$) was calculated using equation (2):

$$k_1 = \frac{k_{app}}{m} \tag{2}$$

where *m* is the mass of AuNX.

### 2.5. Formation of AuNX-PVA nanocomposite hydrogels

Physical PVA-AuNX hydrogels were formed via the widely reported freeze/thaw technique [19, 20]. To assess their catalytic properties, cylindrical hydrogels were formed in a 96-well plate. 300 $\mu$l of aqueous PVA (50 mg ml$^{-1}$) containing 3 $\mu$g AuNX were added to each well and frozen at −20 °C for 1 h before thawing at room temperature thrice. After gelation, the PVA-AuNX hydrogels were removed and stored in water until use.

To evaluate the effect of hydrogel surface area-to-volume ratio, a 300 $\mu$l PVA solution (50 mg ml$^{-1}$) containing 9 $\mu$g of AuNT was added to 3D printed moulds with constant volume but varied dimensions which gave surface area-to-volume ratios between 9–15. After three freeze (at −20 °C) and thaw (at room temperature) cycles, the PVA-AuNT hydrogels were removed from the moulds and stored in ultrapure water until use. The shape and internal dimensions of the moulds were retained by the nanocomposite hydrogels, and so the surface area-to-volume ratio was calculated from the dimensions given above.

For the formation of PVA-AuNT tiles and stacks, an 800 $\mu$l solution of 50 mg ml$^{-1}$/PVA dissolved in pH 4 citrate-phosphate buffer (30.7 mm citric acid and 38.6 mm sodium phosphate dibasic dehydrate) containing, 25 $\mu$g ml$^{-1}$ AuNT was cast into a 3D printed mould with dimensions 20 × 20 × 2 mm. To make the PVA-DAB tiles a 14.4 mg ml$^{-1}$ DAB solution was dissolved in 200 mm HCl. 0.675 ml of the DAB solution was mixed with 3.825 ml of 58 mg ml$^{-1}$ PVA and cast into a mould of the same dimensions. The tiles were frozen at −20 °C for 1 h and thawed at room temperature. After two freeze/thaw cycles, the hydrogel tiles were removed from the moulds and layered to form stacks before a third freeze/thaw cycle.

### 2.6. Catalytic testing of the PVA-AuNX hydrogels

The catalytic performance of the nanocomposite hydrogels was also tested against the reduction of 4-nitrophenol by sodium borohydride. The hydrogels were placed in the 'v'-shaped constriction at the top of Brand Micro UV cuvettes, fully submerged in the catalysis solution, and suspended above the UV–vis spectrometer beam path. Absorbance spectra were collected every 5 min for 30 min, and the reaction kinetics were monitored by the optical absorbance at 400 nm. The reaction rate constants were calculated using equations (1) and (2) as described in section 2.4 and given as the average ± standard deviation of 3 repeats. A fresh hydrogel was used for each repeated measurement.

### 2.7. Assessment of the nano-enzymatic activity of PVA-AuNT hydrogel stacks

The enzymatic activity of the PVA-AuNT nanocomposite stacks was assessed against the oxidation and resultant colour change of DAB by hydrogen peroxide in the presence of a gold catalyst. 2-layer hydrogel stacks were prepared with either PVA-DAB and PVA-AuNT or PVA-DAB, and PVA tiles were placed in Petri dishes with the PVA-DAB layer on the bottom. 2 ml of hydrogen peroxide solution (100, 500, or 1000 mm) was added to the bottom of each dish such that only the PVA-DAB layer of each stack was in contact with the liquid. The stacks were incubated at room temperature for 5 h, and their colour intensity over time was analysed from digital photographs using ImageJ analysis software, as presented as the intensity defined in equation (3):

$$Intensity = (I(t) - I(0)) - (I_{control}(t) - I_{control}(0)) \tag{3}$$

where I(t) and I(0) are the colour intensity at time *t* and time *0* respectively, and $I_{control}(t)$ and $I_{control}(0)$ are the colour intensity in the control sample without hydrogen peroxide at times t and 0.

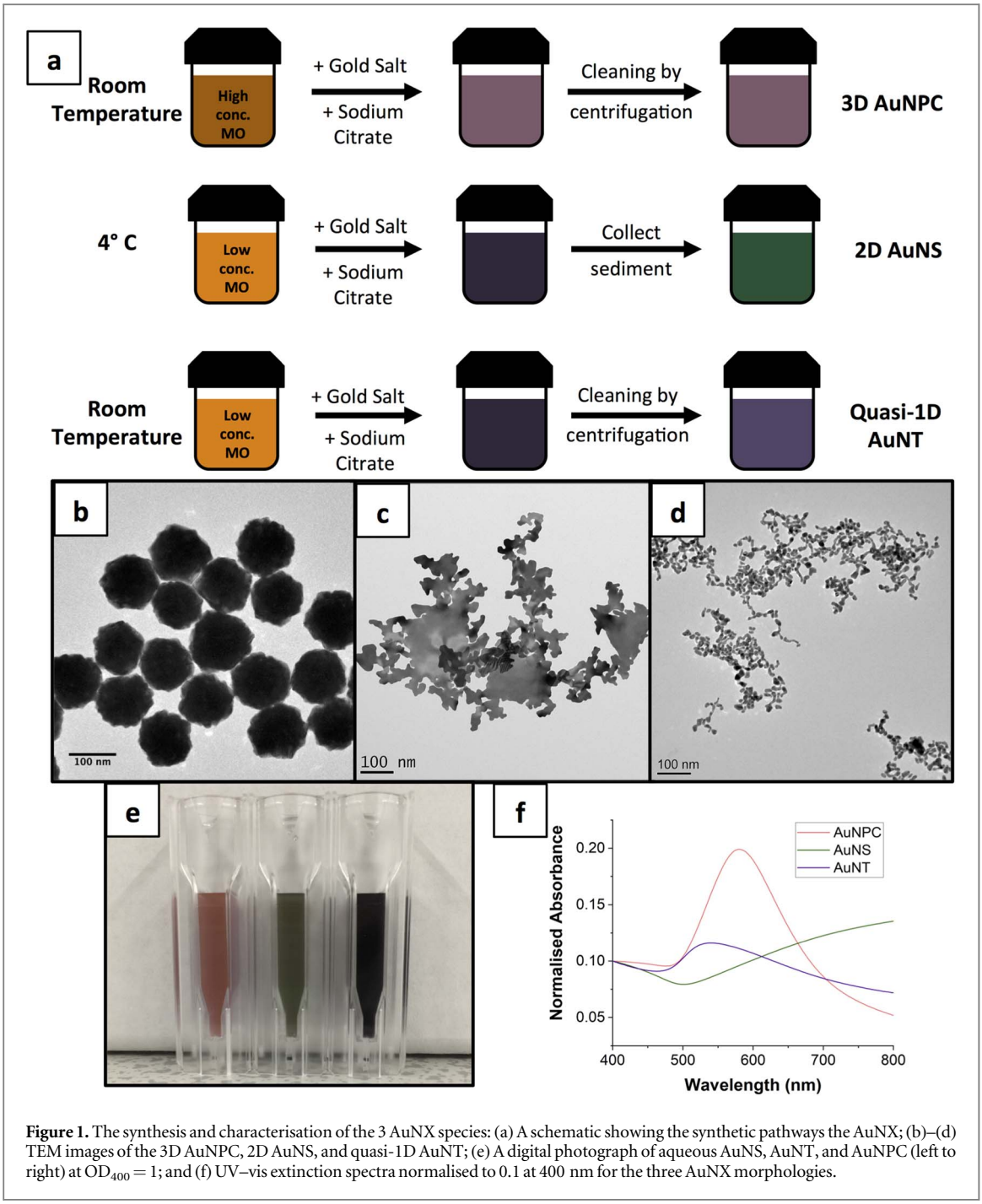


**Figure 1.** The synthesis and characterisation of the 3 AuNX species: (a) A schematic showing the synthetic pathways the AuNX; (b)–(d) TEM images of the 3D AuNPC, 2D AuNS, and quasi-1D AuNT; (e) A digital photograph of aqueous AuNS, AuNT, and AuNPC (left to right) at $OD_{400} = 1$; and (f) UV–vis extinction spectra normalised to 0.1 at 400 nm for the three AuNX morphologies.

## 3. Results and discussion

### 3.1. Synthesis and characterisation of low 3D, 2D, and 1D gold nanoparticles

In this study, 3D, 2D, and quasi-1D gold nanoparticles (collectively termed AuNX) were first prepared. It has been shown previously that the reduction of gold salts by sodium citrate in the presence of methyl orange (MO) leads to the formation of 2-dimensional gold nanosheets (AuNS), where the non-isotropic growth occurs through the strong affinity and adsorption of MO to the (111) plane [8, 18]. Through control of the synthesis temperature and MO concentration, this method has been expanded herein to produce gold NanoPineCones (AuNPC), 3D assemblies of 2D sheets into pinecone structures, and quasi-1D NanoTapes (AuNT) (figure 1(a)).

TEM imaging of the AuNPCs, obtained through a room temperature synthesis with 2.5 mm MO, showed a monodisperse population of nanoparticles with a diameter = 84 ± 29 nm (N = 478; figure 1(b)). These do not have the same planar structures as the 2D AuNS, rather a 3D morphology is observed. We propose that the templating effect of MO led to the formation of small 2D 'flakes', similar to that previously observed in the formation of 2D nanosheets, which was followed by their controlled aggregation and hierarchical assembly. The

flakes were arranged radially and in layers, similar to the petals of a pinecone as found in nature, conferring the high surface area-to-volume ratio of 2D nanostructures. The AuNPCs were found to be highly stable through centrifugation, washing steps, and subsequent storage, without disintegration into their constituent flakes, indicating that they are not simply physical assemblies, rather the flakes in each AuNPC are chemically bound to form a continuous particle. Indeed, the assembly of the precursor flakes during synthesis is likely an intermediary step and was followed by further reduction of gold and rearrangement of atoms. Similar to other gold nanoforms with pseudo-spherical shapes and rough surface topographies, the AuNPC have a pink colour by eye, and a UV–vis extinction peak at 580 nm, red-shifted relative to that of an isotropic sphere [21].

To obtain AuNS, of ~100 nm in diameter and highly fractal edge structures, the MO concentration and synthesis temperature were reduced, to 0.21 mm and 4 °C, respectively. The AuNS synthesis has been discussed previously and produced a solution with a green colour consisting of sheets just two atomic layers thick and with lateral dimension of the order 100 nm (figure 1(c)) [8].

When the 2D synthesis was conducted at room temperature, however, the formation of large AuNS was not observed. Instead, we obtained gold nanotapes (AuNT) that have quasi-1D, tape-like or tadpole-like structures, with a larger 'head ' at one end adjoined to a 2D tape-like region with a flat structure comparable to that seen for the AuNS. The AuNT produced a dark purple colour solution (figure 1(d)) with a peak ca 530 nm, probably associated with the 'head' region and a broad absorption in the IR due to the 2D region. Notably, gold nanospheres or other 3D structures are not observed in the TEM imaging.

### 3.2. The performance of AuNX as heterogeneous catalysts

AuNPs have been employed widely as catalysts. Among them, the morphologies with higher surface area-to-volume ratio have enhanced catalytic rates through the increased availability of gold atoms to the surrounding reaction medium [22–24]. In the case of 2D nanosheets of just 2-atom thickness, where each atom is on the particle surface, this ratio approaches its theoretical maximum. In fact, it is the decrease in dimensionality from 3D to 2D of the nanomaterials, which maximises this ratio and contributes to the exceptional catalytic rates.

It is also known that low coordination atoms at the corners and edges of nanostructures have higher energy and contribute more strongly to the catalytic properties of materials [9]. Under the assumption that a greater perimeter-to-surface area ratio will increase the catalytic activity, we can again hypothesise that rates of catalysis will be a function of dimensionality, where the amount of 'edge' per particle is maximised by the transition from 2D to 1D.

Hence, we evaluated the catalytic performance of the 3D AuNPC, 2D AuNS, and quasi-1D AuNT at a constant mass concentration in the model reduction of nitrophenol (4-NP) by sodium borohydride. Figures 2(a)–(d) shows the UV–vis extinction spectra and resultant kinetics plot collected at 1 min intervals over 5 min where the optical density at 400 nm corresponds to the concentration of 4-NP. With the lowest proportion of surface atoms, the AuNPCs gave the lowest $k_1$ of $4.4 \pm 0.1 \times 10^4$ $min^{-1}$ $g^{-1}$ (figure 2(e)). However, their rough surface topography still offered enhanced catalytic rates over comparably sized gold spheres, which are reported to be $9.2 \times 10^3$ $min^{-1}$ $g^{-1}$ [8]. The increase in surface area-to-volume from a reduction in dimensionality to 2D AuNS gave a nearly 3-fold increase in the rate constant ($k_1 = 11.4 \pm 0.9 \times 10^4$ $min^{-1}$ $g^{-1}$), while the large increase in perimeter-to-surface area (~5-fold; figure 2(f)) caused a 5-fold increase for the 1D AuNTs ($k_1 = 25.7 \pm 0.7 \times 10^4$ $min^{-1}$ $g^{-1}$ ). Although the presence of surface ligands and their density can affect the catalytic properties of nanoparticles [25], the three gold morphologies used here are synthesised from similar methods using the same reducing and templating agents (sodium citrate and methyl orange respectively), so we can assume that the types and density of ligands across their surfaces are comparable. This is particularly true in the case of the 2D AuNS and quasi-1D AuNT, where the synthesis procedure, reagents, and quantities are identical, except for a difference in temperature. Here we can confidently assert that the measured differences in catalytic rate are derived from the particle morphology, not differences in their surface ligands. The measured catalytic rate constant for the AuNTs significantly exceeded that of other freestanding gold nanoparticles reported in the literature, for example, 2D nanosheets ($k_1 = 11.8 \times 10^4$ $min^{-1}$ $g^{-1}$) [22], nanorods ($k_1 = 3.7 \times 10^4$ $min^{-1}$ $g^{-1}$) [26], and nanostars ($k_1 = 1.3 \times 10^4$ $min^{-1}$ $g^{-1}$) [27].

### 3.3. Integration of AuNX into catalytically active nanocomposite hydrogels

The above shows that unsupported gold nanoparticles can provide high catalytic rate constants in aqueous media, but the collection and reuse of 'freely suspended' colloidal catalysts may be non-trivial. Their incorporation into macro-scale hydrogels, however, allows for diffusion of the reaction medium through the gel, and subsequent nanoparticle catalysis without dispersion of the particles into the solvent, thus giving facile collection and recycling. PVA-nanoparticle hydrogel composites, prepared via repeat freeze-thaw cycles, are one such system. The incorporation of nanoparticles into the PVA solution before freezing leads to their uniform

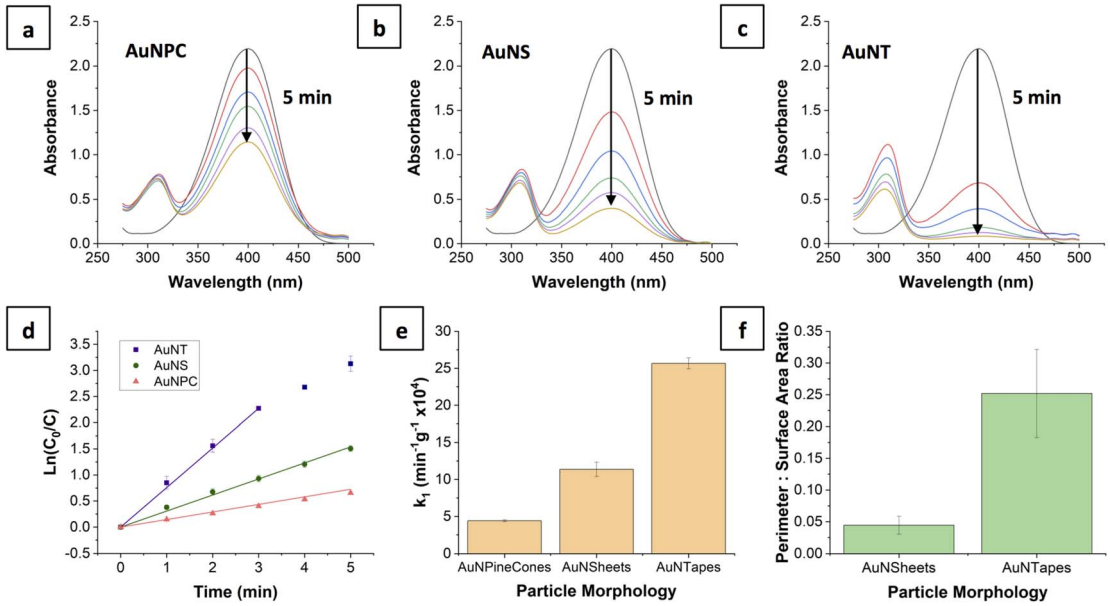


**Figure 2.** Catalytic performance of AuNX in the reduction of 4-nitrophenol by sodium borohydride: (a)–(c) UV-Vs absorption spectra, collected at 5 min intervals for half an hour, of solutions of 4-nitrophenol and sodium borohydride with AuNPC, AuNS, or AuNT respectively; (d) Plots of $Ln(C_0/C)$ against time for the AuNX; (e) the mass normalised catalytic rate constant, $k_1$, for each morphology; and (f) the perimeter : surface area ratio for AuNS and AuNT.

dispersion throughout the matrix [19], and is completed without chemical crosslinkers. Hence, we incorporated each of the three AuNX species into cylindrical PVA hydrogels.

As is seen in figure 3(a), the hydrogels retained the characteristic pink, green, and purple colours of the AuNPCs, AuNS, and AuNTs, respectively, from the high mass concentration of immobilised nanoparticles. The lack of colour change during the freeze/thaw gelation indicates that the PVA stabilised the AuNX species and prevented significant aggregation.

The catalytic performance of the AuNX-PVA nanocomposites was also evaluated for the reduction of 4-NP by sodium borohydride. For measurement, nanocomposites were submerged in solutions of 4-NP and borohydride in plastic cuvettes, suspended above the spectrometer beam path, so kinetic measurements could be taken in real-time. In this regime, catalysis occurred by free diffusion of the 4-NP and borohydride into the hydrogel. Their reaction was catalysed by the AuNX, followed by diffusion back into the bulk medium.

The UV–vis measurements and kinetic plot (figures 3(b)–(e)) show a ~100x decrease in the catalysis rate compared to the freely dispersed AuNX. However, the dependence of catalytic activity on the particle dimensionality is still observed, with an increase from $6.2 \pm 0.7 \times 10^2$ to $1.8 \pm 0.2 \times 10^3$ $min^{-1}$ $g^{-1}$ for AuNPC-PVA and AuNS-PVA hydrogels, and, ultimately the same 5-fold increase to $3.0 \pm 0.1 \times 10^3$ $min^{-1}$ $g^{-1}$ for the AuNT-PVA hydrogels, in good agreement with the trends observed in figure 2. It is clear that despite their incorporation into macro-scale hydrogels, the nanoparticle dimensionality, and hence surface area-to-volume ratio and perimeter-to-surface area ratio, is still integral to the catalytic performance of the AuNX. We propose that the reduction in catalytic activity was due to the slow diffusion of reagents through the hydrogel matrix, causing mass transfer limitations and a diffusion-limited regime. This decreased the availability of unreacted 4-NP and borohydride at the immobilised AuNX as well as diffusion of the product back out of the gel, versus the case of homogeneous catalysis shown above.

### 3.4. Tuning the performance of AuNX-PVA nanocomposite hydrogels

The ~100-fold decrease in the mass normalised catalytic rate constant on incorporating AuNX into nanocomposite PVA hydrogels was believed to be caused by mass transfer limitations from the slow diffusion of analytes into the gel, but could be mitigated by increasing both the concentration of AuNX and the surface area-to-volume ratio of the hydrogels. Figure 4(a) shows the apparent rate constant ($k_{app}$) of 4-NP reduction catalysed by AuNX-PVA hydrogels as a function of the AuNX concentration. In each case, $k_{app}$ increases when the AuNX mass concentration increases from 5 $\mu g$ $ml^{-1}$ to 60 $\mu g$ $ml^{-1}$. This suggests that in this range, the rate of catalysis is inhibited, in part, by the catalytic activity of the immobilised AuNX. However, when the concentration exceeds 60 $\mu g$ $ml^{-1}$ a plateau is reached, where further increase in AuNX concentration has no effect. In this regime, $k_{app}$ is limited purely by diffusion of 4-NP and its reduced product 4-aminophenyl (4-AP) through the hydrogels. Notably, the same trend is observed for each AuNX morphology, supporting the fact that above

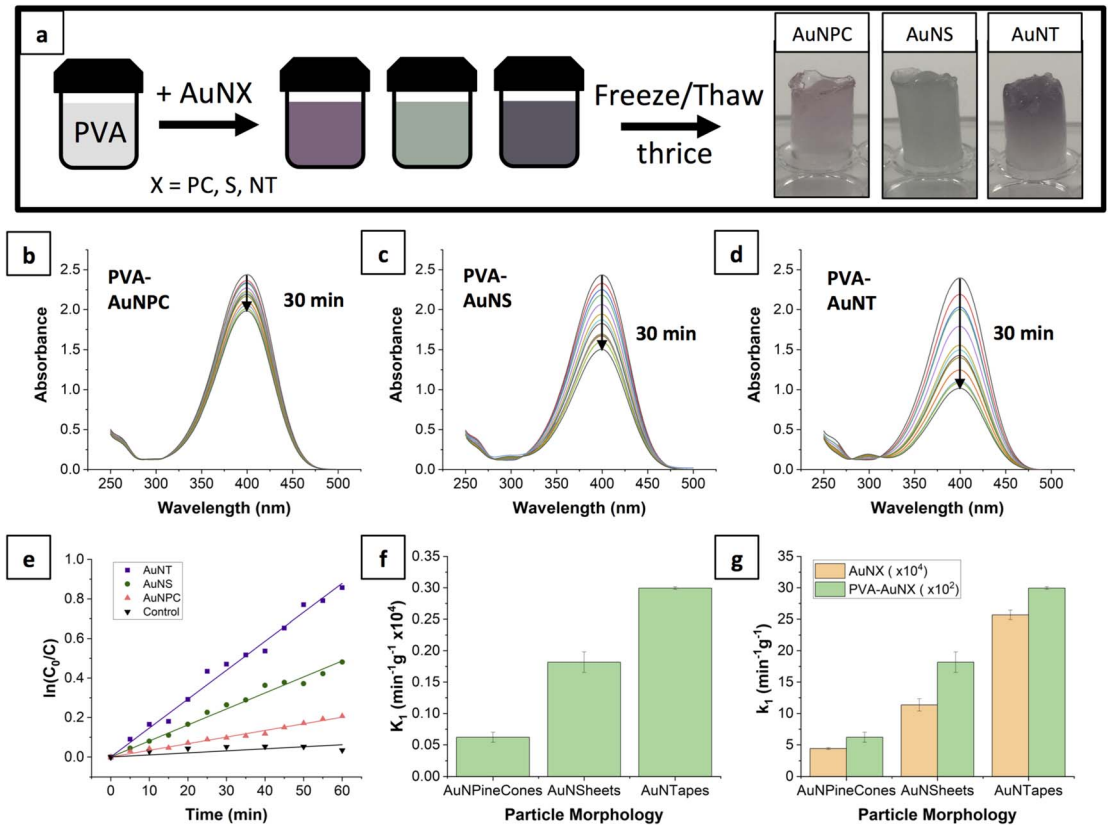


**Figure 3.** The catalytic activity of PVA-AuNX nanocomposite hydrogels: (a) A schematic showing the formation of AuNX-PVA hydrogels; (b)–(d) UV–vis absorption spectra showing the reduction of 4-nitrophenol in the presence of PVA-AuNPC, PVA-AuNS, and PVA-AuNT respectively (5 min interval between scans); (e) $Ln(C_0/C)$ over time for the three hydrogel formulations and a negative control (PVA only); (f) The catalytic rate constants normalised for gold mass, $k_1$, for each hydrogel; and (g) the rate constants compared to those for the AuNX morphologies free in solution.

60 $\mu$g ml$^{-1}$, $k_{app}$ is dominated by diffusion and hence properties of the hydrogel network, not the particle concentration.

When the same data is expressed as the gold mass normalised rate constant, $k_1$, (figure 4(b)) an exponential decay of $k_1$ versus concentration is observed with each morphology converging asymptotically at high concentrations. This highlights the effect of the incorporation of the particles into hydrogels and the resultant need for the diffusion of the reaction mix through the polymer matrix. For particles freely dispersed in an excess of 4-NP, one expects a constant $k_1$. In the nanocomposite hydrogels, where catalysis is in-part diffusion limited, the reaction rate is hindered by the slow mass transfer of 4-NP to and from the catalysis site, and so the rate constant does not increase proportionally with the concentration of the catalyst. While the apparent rate of catalysis ($k_{app}$) increases over this range, the efficiency of the catalysis per unit gold mass decreases.

The influence of diffusion on the catalytic rate may be controlled through the macro-scale geometry of the hydrogel. Figure 4(c) shows $k_{app}$ for 4 PVA-AuNT nanocomposite hydrogels with constant volume and constant gold mass but varied surface area-to-volume ratios. When the dimensions of the hydrogels were small to create a cuboid with a low surface area, the rate of diffusion, and hence mass transfer, to and from the hydrogel was lowest, giving the lowest $k_{app}$ value of 0.008 min$^{-1}$. Changing the dimensions of the hydrogel to provide cuboids of the sequentially higher surface area led to a linear increase in $k_{app}$ to 0.011 min$^{-1}$ with a 1.5-fold increase in surface area. Indeed, at higher ratios, the area through which the 4-NP may diffuse is more extensive, and the distance it must diffuse to reach a gold catalyst is reduced. It is clear that both nano- and macro-scale properties of the gel should be considered when designing nanoparticle-hydrogel nanocomposites for catalytic applications.

### 3.5. Nanocomposite hydrogel tiles for the colourimetric detection of hydrogen peroxide

The hydrophilic polymer networks of hydrogels offer a unique opportunity to perform assays and reactions in a controllable, and facile, manner inside a hydrogel that may be handled, transported, and applied in various environments. To demonstrate the potential utility, we have used the model oxidation of diaminobenzidine (DAB) by hydrogen peroxide in the presence of the quasi-1D AuNTs, which gives a colourimetric change from

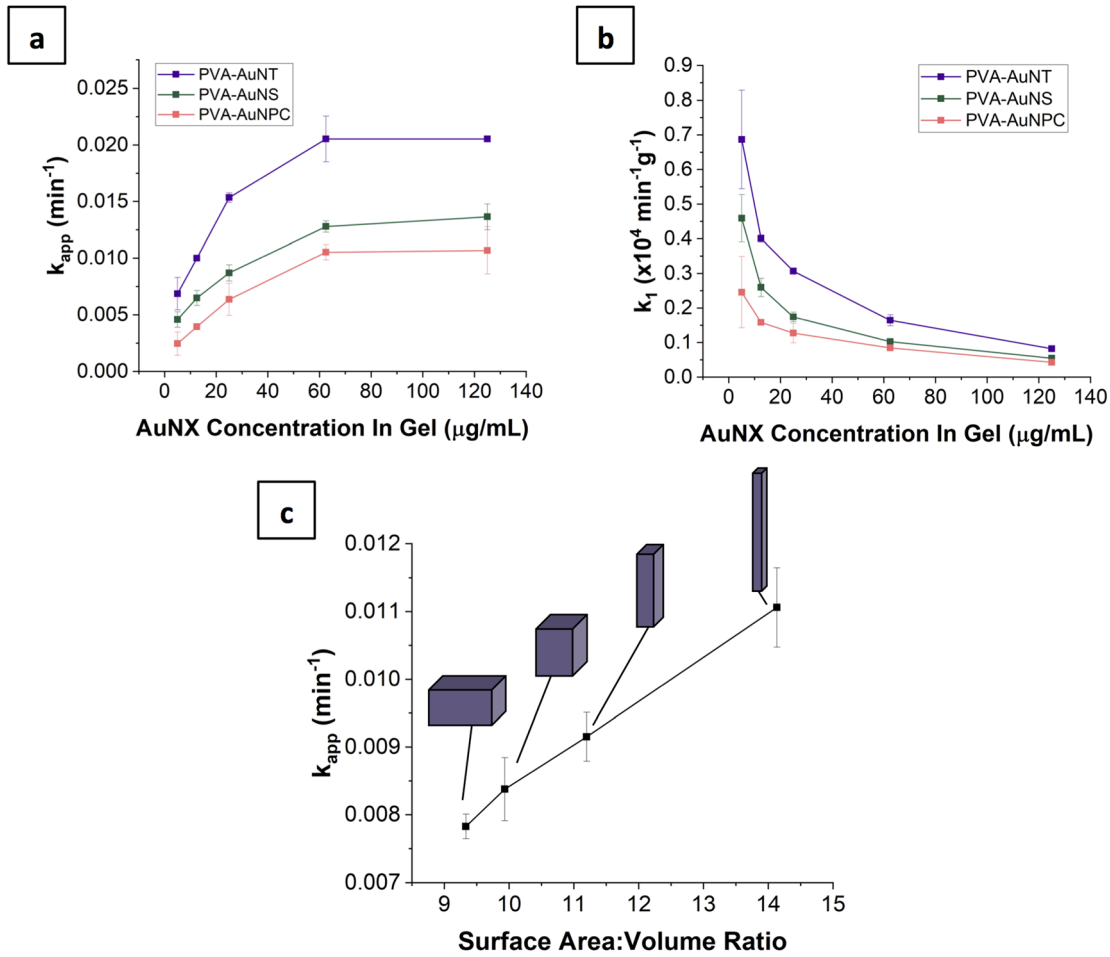


**Figure 4.** Tuning the catalytic performance of PVA-AuNX hydrogels: (a)–(b) the apparent rate constant, $k_{app}$, and mass normalised rate constant, $k_1$, for the PVA-AuNX nanocomposites under varied gold nanoparticle concentration; and (c) $k_{app}$ for PVA-AuNT hydrogels of controlled shape and surface area: volume ratio.

transparent to dark brown. Unlike other reported hydrogel-based flow-through reactors, we employed a modular, multi-layered design here. PVA hydrogels are known to self-heal when their cut surfaces are in intimate contact. The cleavage of bonds creates free hydroxyl groups, which may then re-form hydrogen bonds with adjacent PVA molecules [28]. In this case, however, there is no cleavage of bonds, but it was hypothesised that free hydroxyl groups at the gel surface could 'heal' two hydrogel pieces together without prior cutting.

Firstly, square hydrogel 'tiles' were prepared from freeze-thawed PVA containing either AuNTs or DAB (PVA-AuNT; PVA-DAB), which were then layered on top of each other to form a 'stack'. When the tiles were prepared with just two freeze-thaw cycles, their tensile strength was sufficient for manual handling, and the number of free hydroxyl groups present at the surface was sufficient for 'healing' to the adjacent tile. Notably, Zhang *et al* showed that the strength of a healed join decreases when the surfaces are left out of contact for several hours [28]. The same was true for the tiles and stacks; if left for 24 h without healing together, the tile surfaces became passivated and healing no longer occurred. The crystallisation of the PVA across the tile interface from a third freeze-thaw cycle was used to strengthen the join. The layered nanocomposite stacks could be stretched, bent, and manually manipulated while maintaining a strong physical bond between each tile.

The contact between the adjacent layers was sufficient to allow the diffusion of molecules between the tiles. When placed in a hydrogen peroxide solution (such that the liquid level did not rise above the first tile), the peroxide could diffuse through the bottom PVA-DAB layer and up into the PVA-AuNT tile (figure 5(a)). This liquid diffusion through the lower layer was also sufficient to transport the DAB into the upper AuNT-PVA tile. When both the DAB substrate and the $H_2O_2$ were present in the upper tile, the oxidation of DAB was catalysed due to the presence of the AuNTs, causing the formation of DAB precipitate and an associated colour change from transparent to dark brown. Notably, the use of separate modular tiles allowed for the preparation of reagents under different solvent conditions. In this case, a highly acidic environment was required to dissolve the DAB and prepare the PVA-DAB tile. In contrast, the PVA-AuNT was prepared with a citrate-phosphate buffer at pH 4, for optimum catalytic activity. These two different pH regimes could not have been achieved using a

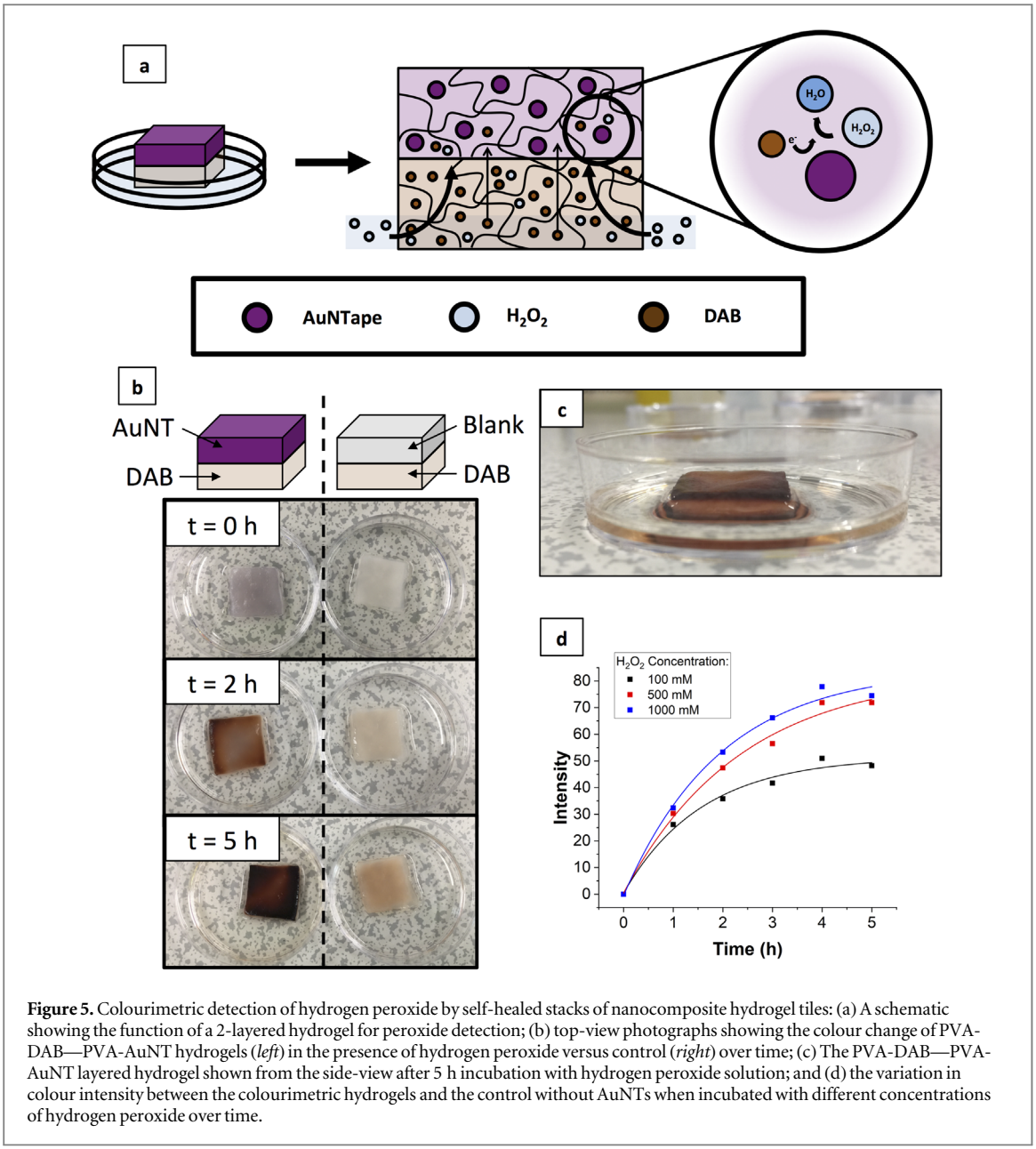


**Figure 5.** Colourimetric detection of hydrogen peroxide by self-healed stacks of nanocomposite hydrogel tiles: (a) A schematic showing the function of a 2-layered hydrogel for peroxide detection; (b) top-view photographs showing the colour change of PVA-DAB—PVA-AuNT hydrogels (*left*) in the presence of hydrogen peroxide versus control (*right*) over time; (c) The PVA-DAB—PVA-AuNT layered hydrogel shown from the side-view after 5 h incubation with hydrogen peroxide solution; and (d) the variation in colour intensity between the colourimetric hydrogels and the control without AuNTs when incubated with different concentrations of hydrogen peroxide over time.

conventional, single hydrogel system. Figure 5(b) shows how the stack performed as a colourimetric assay to detect hydrogen peroxide, where the colour change from purple (from the AuNT present in the upper tile) to dark brown was seen by eye. While some auto-oxidation of DAB and colour change was observed in the control sample after 5 h of submersion in the peroxide solution, the colour change is negligible compared to the stack containing the PVA-AuNT layer.

A lateral view of the PVA-DAB—PVA-AuNT stack after incubation in hydrogen peroxide for 5 h showed that the colour change occurred in the top layer, in agreement with the proposed mechanism of diffusion of hydrogen peroxide upwards through the tiles. The colour change was also seen through the full depth of the top PVA-AuNT tile, not just at the interface with the lower PVA-DAB layer, confirming that the DAB also diffuses into the upper tile (figure 5(c)). Minimal colour change was seen in the PVA-DAB layer and surrounding liquid. This suggests the formation of large DAB precipitates during their oxidation which inhibits their diffusion back into the lower tile and the medium, confining the colour change to the PVA-AuNT tile. Notably, after use, the stacks showed no loss of structural integrity and could still be handled, stretched, and bent without breakage at the join between adjacent tiles.

Image analysis of photographs of the nanocomposite stacks was used to quantify the colour change over time at different concentrations of hydrogen peroxide (figure 5(d)). Higher concentrations of peroxide caused greater oxidation of the DAB after diffusion into the top PVA-AuNT layer, resulting in a more intense colour change relative to the control. Initially, the upper tile has no DAB or peroxide and may be considered a 'sink', allowing

for their rapid diffusion and fast reaction rate and colour change up to 1 h. Over larger timescales, the concentrations of peroxide and DAB across the tiles equilibrate, and unreacted species are depleted, slowing the continued oxidation of DAB and causing a plateau in colour change. The constant colour change implies continued diffusion of molecules across the interface over the full experiment time. After 5 h, a clear difference was observed between the different peroxide concentrations showing that the nanocomposite stacks could be used for a qualitative comparison between samples.

## 4. Conclusion

Our studies have demonstrated that reducing the dimensionality of gold from 3D nanoparticles to 2D sheets and tapes improves their catalytic and enzymatic properties. Further, the improvement observed between the 2D sheets and the quasi-1D tapes indicates that the 'edges' are most likely responsible for the catalytic activity. Embedding the different AuNX morphologies into hydrogels restrained their mobility whilst maintaining their activity. However, the observed catalytic and enzymatic activity was significantly reduced compared to free AuNX due to reduced diffusion, slowing the uptake of the substrate and analytes into the gel. Notwithstanding this, by creating thin gels with higher surface-to-volume ratios, the rate of enzymatic activity can be increased significantly. Further, we have demonstrated that it is possible to create composite hydrogel structures where tiles with different functional entities can be effectively bonded and retain their ability to transport substrates and reagents between layers—opening new possibilities for enzymatic-based diagnostic devices and reusable catalysts.

## Acknowledgments

J F is supported by a philanthropic donation from Excel Communications. GN and S D E acknowledge support from the NTI funding the University of Leeds. S D E was supported by the National Institute for Health Research (NIHR) infrastructure at Leeds. The FEI Tecnai G2-Spirit (T12) used for TEM imaging was funded by The Wellcome Trust (090932/Z/09/Z).

## Data availability statement

The data that support the findings of this study are openly available at the following URL/DOI: https://doi.org/10.5518/1294.

## ORCID iDs

George Newham https://orcid.org/0000-0002-4877-5513
Stephen D Evans https://orcid.org/0000-0001-8342-5335

## References

[1] Gao L *et al* 2007 Intrinsic peroxidase-like activity of ferromagnetic nanoparticles *Nat. Nanotechnol.* **2** 577–83
[2] Yang W, Yang X, Zhu L, Chu H, Li X and Xu W 2021 Nanozymes: activity origin, catalytic mechanism, and biological application *Coord. Chem. Rev.* **448** 214170
[3] Liang M and Yan X 2019 Nanozymes: from new concepts, mechanisms, and standards to applications *Acc. Chem. Res.* **52** 2190–200
[4] Zhang Y, Villarreal E, Li G G, Wang W and Wang H 2020 Plasmonic nanozymes: engineered gold nanoparticles exhibit tunable plasmon-enhanced peroxidase-mimicking activity *J. Phys. Chem. Lett.* **11** 9321–8
[5] Liu B, Han X and Liu J 2016 Iron oxide nanozyme catalyzed synthesis of fluorescent polydopamine for light-up zn2+ detection *Nanoscale* **8** 13620–6
[6] Pedone D, Moglianetti M, Lettieri M, Marrazza G and Pompa P P 2020 Platinum nanozyme-enabled colorimetric determination of total antioxidant level in saliva *Anal. Chem.* **92** 8660–4
[7] Geng X, Xie X, Liang Y, Li Z, Yang K, Tao J, Zhang H and Wang Z 2021 Facile fabrication of a novel copper nanozyme for efficient dye degradation *ACS Omega* **6** 6284–91
[8] Ye S *et al* 2019 Sub-nanometer thick gold nanosheets as highly efficient catalysts *Adv. Sci.* **6** 1900911
[9] Kim S *et al* 2021 Correlating 3d surface atomic structure and catalytic activities of pt nanocrystals *Nano Lett.* **21** 1175–83
[10] Schmieg B, Döbber J, Kirschhöfer F, Pohl M and Franzreb M 2019 Advantages of hydrogel-based 3d-printed enzyme reactors and their limitations for biocatalysis *Front. Bioeng. Biotechnol.* **6** 1–12
[11] Kudaibergenov S E and Dzhardimalieva G I 2020 Flow-through catalytic reactors based on metal nanoparticles immobilized within porous polymeric gels and surfaces/hollows of polymeric membranes *Polymers* **12** 572
[12] Mai A Q, Bánsági T, Taylor A F and Pojman J A 2021 Reaction-diffusion hydrogels from urease enzyme particles for patterned coatings *Commun. Chem.* **4** 1–7

[13] Wang S, Zheng H, Zhou L, Cheng F, Liu Z, Zhang H, Wang L and Zhang Q 2020 Nanoenzyme-reinforced injectable hydrogel for healing diabetic wounds infected with multidrug resistant bacteria *Nano Lett.* **20** 5149–58
[14] Zhao Y, Song S, Wang D, Liu H, Zhang J, Li Z, Wang J, Ren X and Zhao Y 2022 Nanozyme-reinforced hydrogel as a h2o2-driven oxygenerator for enhancing prosthetic interface osseointegration in rheumatoid arthritis therapy *Nat. Commun.* **13** 1–14
[15] Li Z *et al* 2022 A nanozyme-immobilized hydrogel with endogenous ros-scavenging and oxygen generation abilities for significantly promoting oxidative diabetic wound healing *Adv. Healthc. Mater.* **2201524** 1–16
[16] Ko E, Hur W, Son S E, Seong G H and Han D K 2021 Au nanoparticle-hydrogel nanozyme-based colorimetric detection for on-site monitoring of mercury in river water *Microchim. Acta* **188** 382
[17] Baretta R, Gabrielli V and Frasconi M 2022 Nanozyme-cellulose hydrogel composites enabling cascade catalysis for the colorimetric detection of glucose *ACS Appl. Nano Mater.* **5** 13845–53
[18] Fox J, Newham G, Bushby R J, Valleley E M A, Coletta P L and Evans S D 2023 spectrophotometric analysis and optimization of 2d gold nanosheet formation *J. Phys. Chem.*C **127** 3067–76
[19] Yao S, Zhou C and Chen D 2013 A highly porous PVA dried gel with gold nanoparticles embedded in the network as a stable and ultrasensitive SERS substrate *Chem. Commun.* **49** 6409–11
[20] Stauffer S R and Peppast N A 1992 Poly(Vinyl Alcohol) hydrogels prepared by freezing-thawing cyclic processing *Polymer (Guildf).* **33** 3932–6
[21] López-Muñoz G A, Pescador-Rojas J A, Ortega-Lopez J, Salazar J S and Abraham Balderas-López J 2012 Thermal diffusivity measurement of spherical gold nanofluids of different sizes/concentrations *Nanoscale Res. Lett.* **7** 1–6
[22] Baral A, Cavalieri F, Chattopadhyay S and Ashokkumar M 2021 Synthesis of gold nanosheets with controlled morphology by combining a natural amino acid with high-frequency ultrasound *ACS Sustain. Chem. Eng.* **9** 13953–62
[23] Cui Q, Xia B, Mitzscherling S, Masic A, Li L, Bargheer M and Möhwald H 2015 Preparation of gold nanostars and their study in selective catalytic reactions *Colloids Surfaces A Physicochem. Eng. Asp.* **465** 20–5
[24] Deshmukh A R and Kim B S 2021 Flower-like biogenic gold nanostructures for improved catalytic reduction of 4-nitrophenol *J. Environ. Chem. Eng.* **9** 106707
[25] Vargas K M, San K A and Shon Y S 2019 Isolated effects of surface ligand density on the catalytic activity and selectivity of palladium nanoparticles *ACS Appl. Nano Mater.* **2** 7188–96
[26] Gao D *et al* 2016 Morphology-selective synthesis of active and durable gold catalysts with high catalytic performance in the reduction of 4-nitrophenol *Nano Res.* **9** 3099–115
[27] Ndokoye P, Zhao Q, Li X, Li T, Tade M O and Wang S 2016 Branch number matters: promoting catalytic reduction of 4-nitrophenol over gold nanostars by raising the number of branches and coating with mesoporous SiO2 *J. Colloid Interface Sci.* **477** 1–7
[28] Zhang H, Xia H and Zhao Y 2012 Poly(Vinyl Alcohol) hydrogel can autonomously self-heal *ACS Macro Lett.* **1** 1233–6